Lasers in Eng., Vol. 46, pp. 343–357
Reprints available directly from the publisher
Photocopying permitted by license only

Debris-free Cutting of Quartz with Zero Kerf Width and Ultra-low Surface Roughness Using Femtosecond Bessel Laser Beam Filamentation

Z-Q. LI[1], W. GUO[1], O. ALLEGRE[1], C-G. LIU[3], W-Y. GAO[2], X-F. WANG[2], Z-X. HOU[2], K. LI[2], L. ZHANG[2] AND L. LI[1,*]

[1]*Laser Processing Research Centre, Department of Mechanical, Aerospace and Civil Engineering, The University of Manchester, Oxford Road, Manchester, M13 9PL, UK*
[2]*Beijing Institute of Aerospace Control Devices, 52 Yongdong Road, Beijing 100039, China*
[3]*Department of Mechanical, Aerospace and Civil Engineering, The University of Manchester, Oxford Road, Manchester, M13 9PL, UK*

Quartz is a hard and brittle material that is difficult to cut with mechanical tools without generating microcracks and debris, leading to potential weakening of the material and scratches. Herein we present the findings of an investigation into high quality quartz (JKS2) cutting with high uniformity and repeatability using a Ti:Sapphire femtosecond pulse non-diffraction zero order Bessel laser beam filamentation to induce a change in material refractive index followed by mechanical cleavage. The Bessel beam was generated by passing the laser beam through an axicon lens with a physical angle of 20.0°. Our experimental results show that vertical wall stealth dicing can be achieved with workpiece thicknesses of 0.5 mm and 1 mm with a zero cut kerf width and with no debris or microcracks on the cut surface. The cut surface roughness was below 340 nm Ra. The effects of pulse energy and scanning speed of Bessel beam on cleavage force and sidewall surface roughness were discussed.

Keywords: Ti:Sapphire femtosecond laser, quartz, (JKS2, non-diffraction, zero order, Bessel beam, stealth dicing, filamentation

*Corresponding author: E-mail: lin.li@manchester.ac.uk

1 INTRODUCTION

Cutting technologies for transparent materials such as quartz have attracted much attention in the electro-optical industries. Due to its unique characteristics including anti-corrosion, low dielectric loss and high optical transmission, quartz is widely applied in consumer electronics manufacture such as the manufacturing of mobile phones and displays. Traditionally methods such as mechanical wheel cutting and diamond tool-based scoring and break methods [1] create poor near surface finish with microcracks leading to reduced product life. Post processing such as grinding and polishing are required to achieve smooth surfaces. Advanced glass cutting methods such as water jet cutting [2], hot air jet cutting [3], and laser cutting [4] have been developed and used for decades. Water jet cutting creates no heat affected zones due to the flowing water. This technology is divided into abrasive and nonabrasive methods for different smoothness requirements. However, due to the use of abrasive materials, water and water jet nozzles increase the production cost. Alternative methods such as hot air jet-based cutting could produce smoother cuts through nonuniform heating leading to directional thermal stresses followed with controlled crack propagation. The limitation of this technique is that a scratch at the edge of the glass is required to initiate the crack propagation, resulting in weakening of the edge.

Laser based glass cutting can be achieved using four different methods: laser scribing and breaking, controlled fracture propagation, laser melting and evaporation, and short or short-pulse laser ablation [5]. Laser scribe and break method is similar to the traditional glass cutting method. A laser beam, such as a CO_2 laser beam, is applied to generate a groove at a depth of one third to one half of the glass sheet thickness, then a braking force is applied to break the glass along the groove. The scribing process typically induce defects to the cut surface, and thus post processing is required. Controlled fracture propagation is carried out by applying a CO_2 or an Nd:YAG laser or a diode/fibre laser. Similar to the hot air jet method, an initial crack is necessary. Laser beam is applied to generate a compressive stress. After the natural cooling or through a rapid cooling system, a local residual tensile stress is induced. Crack propagation is initiated when the stress exceeds the glass failure stress. Cutline deviation near the end edge was identified [6]. Laser melting and evaporation uses a CO_2 laser to melt and vaporise the glass. Due to the poor edge quality, polishing and grinding is normally required in a post processing stage.

Over the last 15 years, nanosecond, picosecond and femtosecond pulsed lasers have been used for precision cutting of glass. By focusing a laser beam at the bottom surface of the glass, a channel of microcracks can be generated and propagated upward to the top surface after a multiple scanning. This technology is only feasible for cutting thin glass materials and microcracks are typically generated on the cut surface. Ultrashort (picosecond or femto-

second) pulse laser beams can be applied for stealth cutting (zero width, no damage). Due to the non-linear absorption of a ultrashort pulse laser, materials such as quartz can be processed even though the material is transparent at the laser wavelengths [7]. Stealth dicing can be achieved through the highly localized material property modification. The method to realise stealth dicing includes the generation of dotted lines [8], elongated spots [9], and laser filamentation [10, 11].

This paper reports an investigation into the cutting and cleavage of quartz plates using a non-diffraction, femtosecond-pulse Bessel laser beam with excellent uniformity and the long depth of focus. Thanks to the non-diffracting Bessel beam, the femtosecond laser beam was focused with a non-diverging, long depth of focus inside of the quartz material. The effects of pulse energy and scanning speed of Bessel beam on the 1.0 and 0.5 mm thickness quartz cleavage were investigated. Based on laser modification of refractive index followed by mechanical cleavage, both straight and curves cutting were achieved with vertical kerfs (zero taper), no microcracks or no debris are generated, and without any chemicals involved.

2 EXPERIMENTAL METHODOLOGY

The laser used was a Ti:Sapphire femtosecond laser (LIBRA Ti:Sapphire; Coherent, Inc.) system having an 800 nm wavelength with a 100 femtosecond pulse duration, a 1 kHz maximum repetition rate, M^2<1.5, an output power of up to 1 W, with a raw beam diameter of 5 mm. Neutral density filters were applied to controlling the pulse energy. A half waveplate and a polarization filter were applied to controlling the pulse energy and the linear polarization direction. A quarter waveplate was applied to transform the linear polarization into circular polarization, in order to avoid the uneven processing. A non-diffraction zero order Bessel beam was generated by focusing the normal Gaussian beam through a high quality fused silica axicon lens with a physical angle, α of 20.0° (Thorlabs, Inc.) in the manner described by Duocastella *et al.* [12], producing high aspect ratio uniform filamentation in the workpiece. A quartz wafer (JKS2) sheet of 1 mm in thickness was placed on a three-axis translation computer numerical control (CNC) stage (ALS130-150; Aerotech, Inc.). The experimental arrangement is shown in Figure 1.

Based on the physical angle of axicon lens being α=20.0°, the deflection angle of the generated Bessel beam can be obtained using [13]

$$n \sin \alpha = \sin(\alpha + \beta) \tag{1}$$

where the refractive index n of fused silica at 800 nm wavelength light is 1.4533. The deflection angle of the generated Bessel beam, , can be obtained

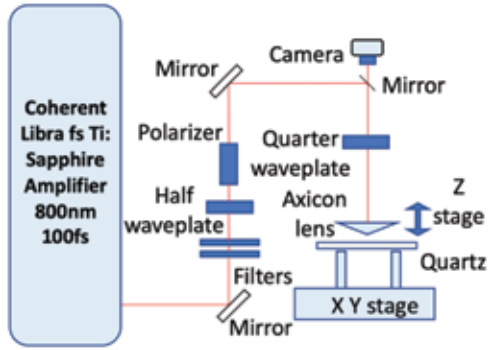

FIGURE 1
Schematic representation of the experimental arrangement.

as 9.8°. One can calculate the central core diameter and the central core length, based on [14]

$$r = \frac{1.2024\lambda}{\pi \sin\beta} \tag{2}$$

and

$$L = \frac{\omega_o}{2\tan\beta} \tag{3}$$

The central core diameter (the focused laser beam diameter) and the central core length (depth of focus) were calculated to be 1.8 and 14.5 mm, respectively. The typical pattern of the focused femtosecond laser beam in the focal region is shown in Figure 2(a) and Figure 2(b). Figure 2(c) and Figure 2(d) show the focused intensity produced with a Bessel beam under the same conditions as those used in our experiments. The diameter of the central core in full width at half maximum (FWHM) was about 1.7 μm, which is consistent with the theoretical calculations. Focusing through the axicon lens generated axially symmetric interference of plane waves, producing a high intensity central with lower intensity concentric rings surround it [15].

The quartz wafer plate was placed on the central area of the Bessel beam focal range. The laser intensity of the surrounding lower intensity concentric rings did not exceed the optical breakdown threshold, so that it would not affect the cutting process. By moving the workpiece relative to the Bessel beam, patterns were generated through the thickness of the workpiece.

After the femtosecond laser inscription, mechanical forces were applied to cleave the material to realise stealth dicing. As shown in Figure 3, a micro test

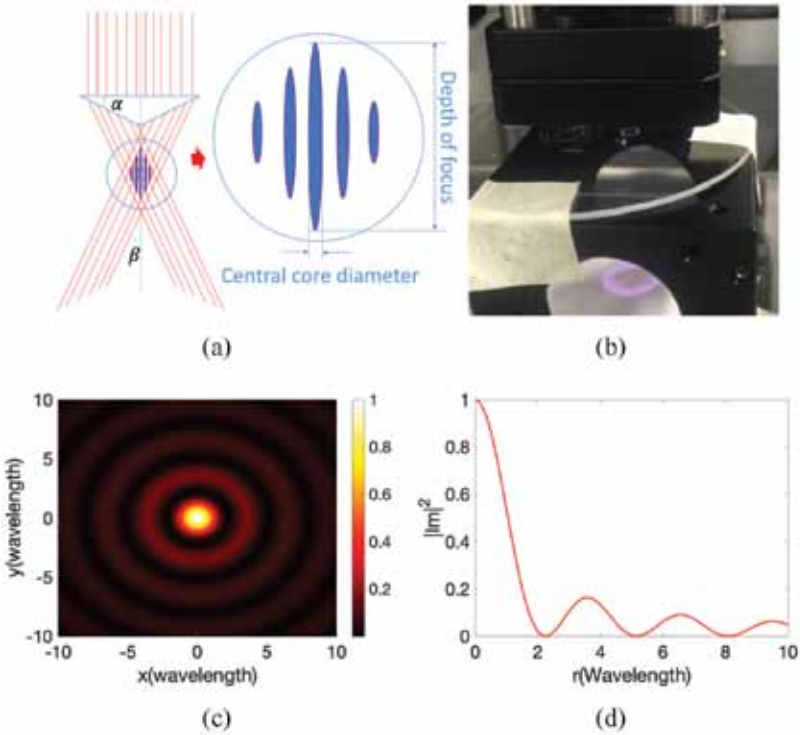

FIGURE 2
(a) Schematic representation of the focused Bessel beam showing typical interference patterns produced in the focal region (inset), (b) Experimental Bessel beam focusing and simulated Bessel beam intensity profiles induced in the focal region, (c) within the *x*-*y* focal plane and (d) normalized to the peak intensity.

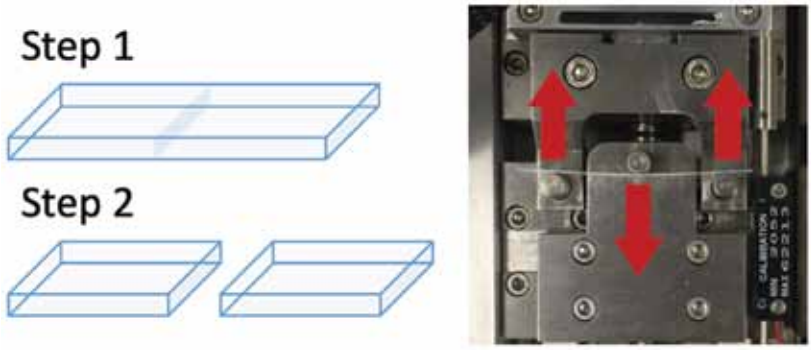

FIGURE 3
Bessel beam cutting and cleavage illustration (left-hand side) and the actual device used in this work (right-hand side).

machine (5 kN Tensile Tester; Deben UK, Ltd.) was applied for bending the quartz with a thickness of 1.0 and 0.5 mm. Sample analysis was conducted with a scanning electron microscope (SEM) (Ultra 55; Carl Zeiss AG). Before the samples were observed under the SEM a 10 nm thick Au/Pd coating was applied to make the surfaces conductive. The sidewall quality was analysed with a white light interferometer (WLI) (Contour GT-K; Veeco Instruments, Inc.) and an optical microscope (VHX 5000; Keyence Corporation).

3 RESULTS AND DISCUSSION

3.1 Bessel beam filamentation

Figure 4 shows the top view of Bessel beam processing results, with 550 μJ pulse energy, scanning speeds from 0.5 to 9.0 mm/s. It can be seen that by increasing the scanning speed, the laser pulses could be separated and the width of the line reduced. The diameter of single pulse was around 1.75 μm, which is quite close to the calculated value. With an increase of the scanning speed, the filamentations were separated, so that the refractive index change near the surface, as shown in Figure 4(e), became weaker. When the scanning speed was further increased, the filamentation would gradually fade. When the pulse energy was reduced, the refractive index change also disappeared gradually and only left the ablation result on both top surface and bottom surface.

These results are attributed to the way the femtosecond laser Bessel beam interactions with the transparent material, by multi-photon absorption [16]. During the femtosecond pulse Bessel beam-material interaction, the processed material near the top or bottom surface were expanded and evaporated, whereas the material in the central area had no space to be dispelled, thus the rapid heating in the filamentation zone induced a refractive index change and weakened region along the specific cut paths. Applying a mechanical force along these paths after laser processing resulted in material cleavage.

To verify this statement, a quartz sheet was processed by using Bessel beam to generate a cross-cutting. Conducting mechanical cleavage in one of cuts, the cross section of the r cut can be observed. Figure 5(a) shows an overall cross-section of the Bessel beam processing (550 μJ pulse energy, 1 mm/s scanning speed). It can be seen that a cutting contour through the thickness of the quartz was generated. An enlarged picture can be observed in Figure 5(b) and Figure 5(c). It can be noticed that the contour is actually disconnected, in some area, the cutting made the sample separated (red arrows), in the other area, the material was solidified and connected again (purple arrows). Also, microstructures can be observed on the sidewall (orange dotted circles) after the mechanical cleavage. It is consistent with the above statements. Similar solidified phenomenon has been observed during Bessel beam drilling [17].

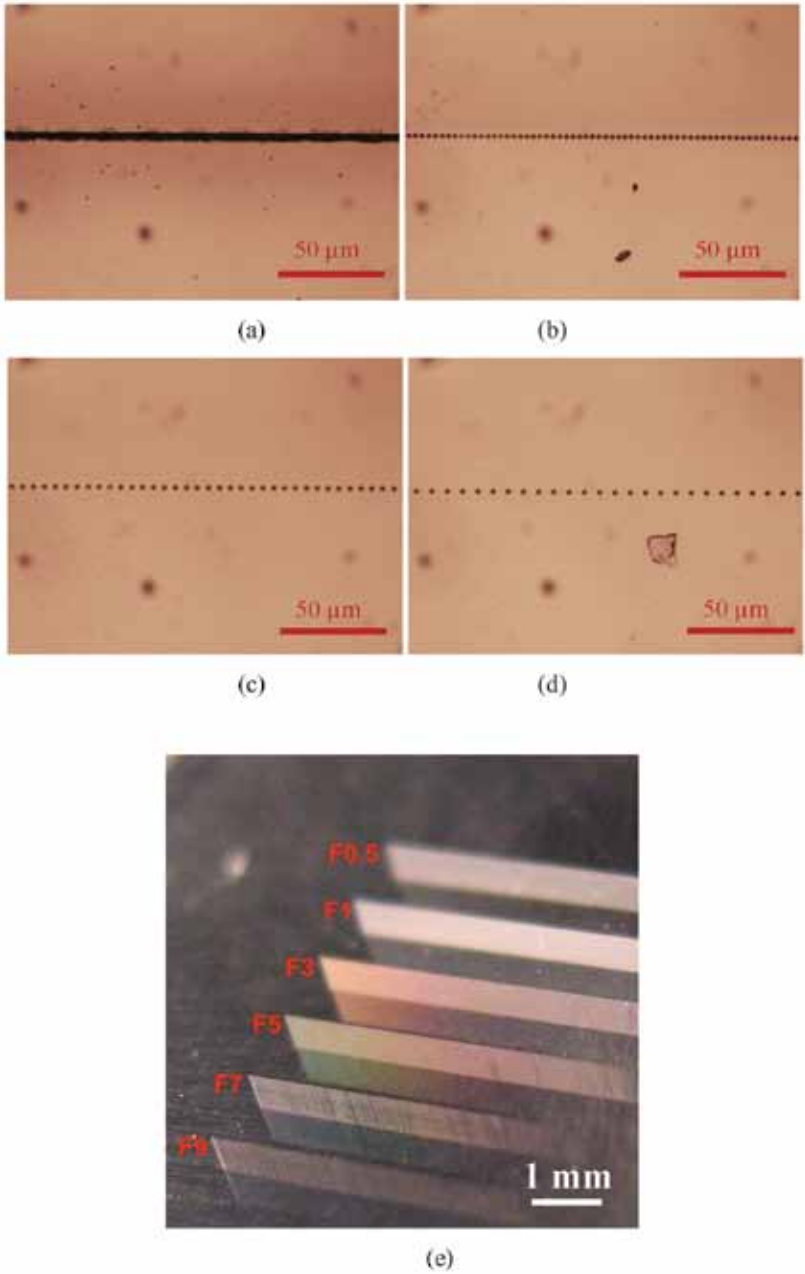

FIGURE 4
Optical micrographs showing the refractive index modification induced with a Bessel beam into a 1.0 mm thick quartz workpiece. Top views are shown where the scanning speeds were (a) 1 mm/s, (b) 3 mm/s, (c) 5 mm/s and (d) 7 mm/s, and (e) micrographs of Bessel beam generated filamentation in quartz with different scanning speeds and taken at 45° angles.

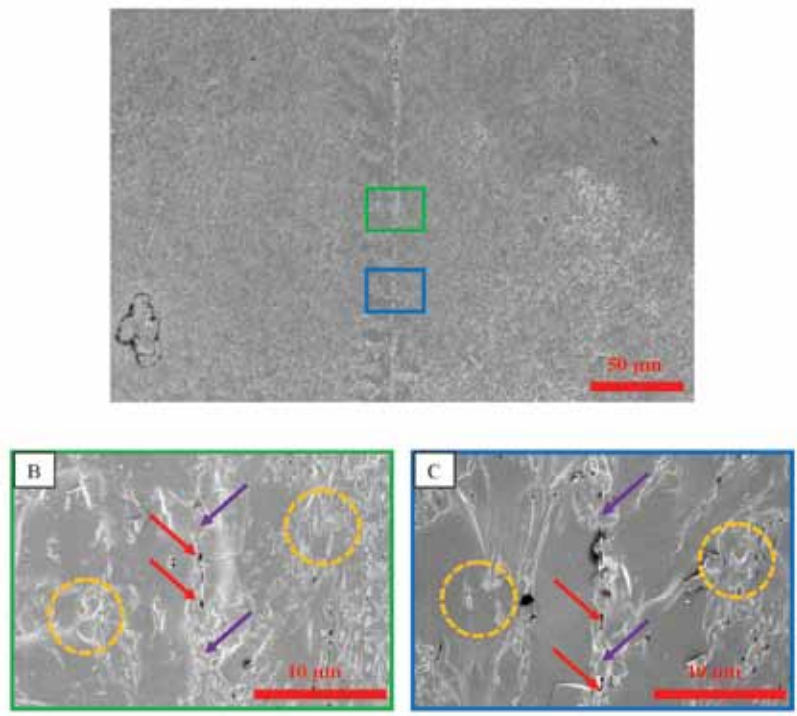

FIGURE 5
SEM micrographs of the quartz sheet Bessel beam cutting cross section with magnifications of (a) 1000×, and (b) and (c) 10000×.

3.2 Cut surface quality

After Bessel beam processing, the cleavage was completed by using a micro bending test machine. Quartz sheets with thickness of 1.0 and 0.5 mm were separated into 50×10 mm^2 size with high quality sidewalls to avoiding crack generation duration bending testing. The three-point bending test strategy is shown in Figure 3. The distance between the first point and the third point was 35 mm. Setting the motor speed to be 0.01 mm/s. With 550 and 400 μJ pulse energy and a scanning speed ranging from 0.5 to 9.0 mm/s, the bending forces for the cleavage were measured and plotted as shown in Figure 6 and Figure 7.

It was found that with the increase of scanning speed, bending force for cleavage was generally increased. The smallest bending force for the 1.0 and 0.5 mm thick quartz plates were 6.8 and 1.4 N, respectively, under 550 μJ pulse energy; and was 10.0 and 2.7 N, respectively, under 400 μJ. A decrease of the bending force at low scanning speeds of 1.0 to 3 mm/s under 550 μJ meant that cutting at a lower scanning speed may have generated more damage to the cut paths, which would increase the surface roughness.

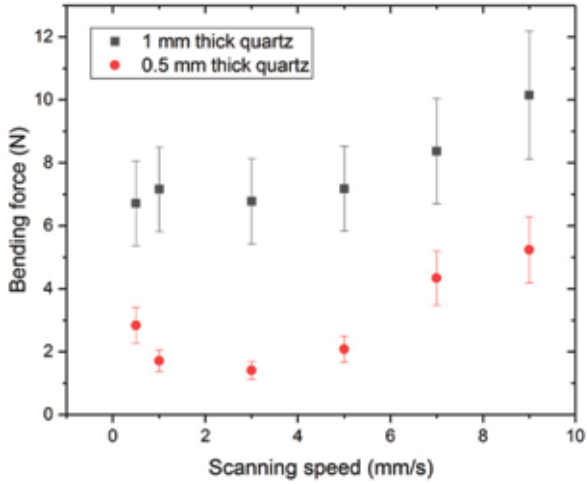

FIGURE 6
Graph showing the quartz sheet bending force for laser cut samples using 550 μJ pulse energy with different scanning speeds.

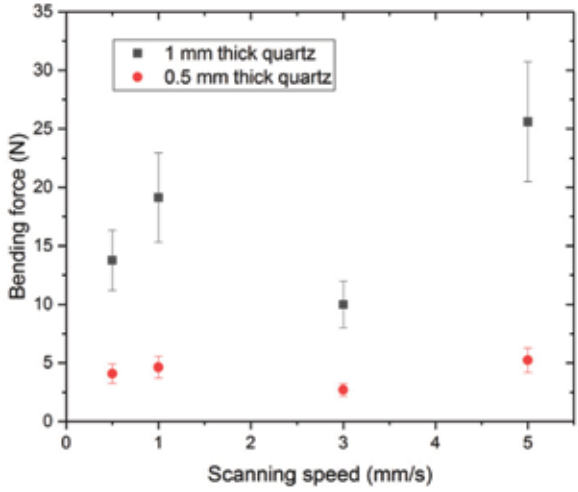

FIGURE 7
Graph showing the quartz sheet bending force for laser cut samples at 400 μJ pulse energy with different scanning speed.

After the three-point bending the cut surface roughness of the sidewalls was measured and analysed using the WLI. Under the 10× objective lens measurement, an 860 × 650 μm^2 area was measured, as shown in Figure 8. The trend of surface roughness under different scanning speed are shown in Figures 9 to 12.

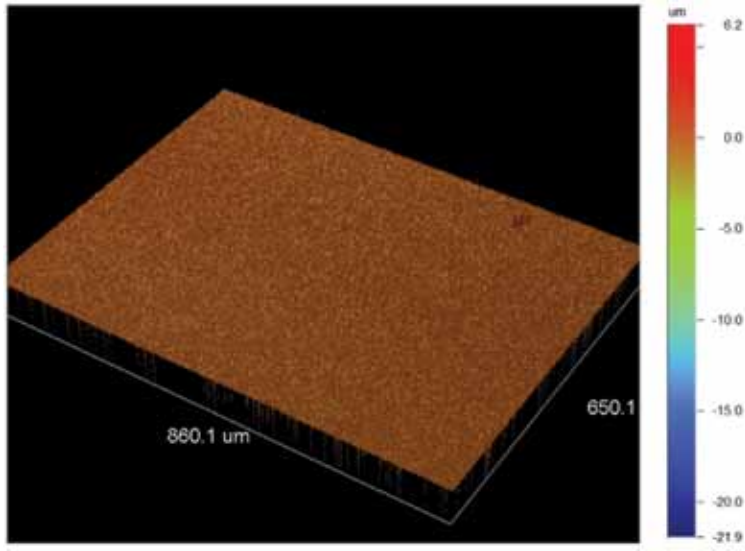

FIGURE 8
WLI surface measurement image.

From Figure 9 and Figure 10 it can be found that under 550 μJ pulse energy, the smallest surface roughness was at around 4 mm/s. The lowest surface roughness were 331 nm Ra and 319 nm Ra for the 1.0 and 0.5 mm thickness, respectively. At this scanning speed the pulses were

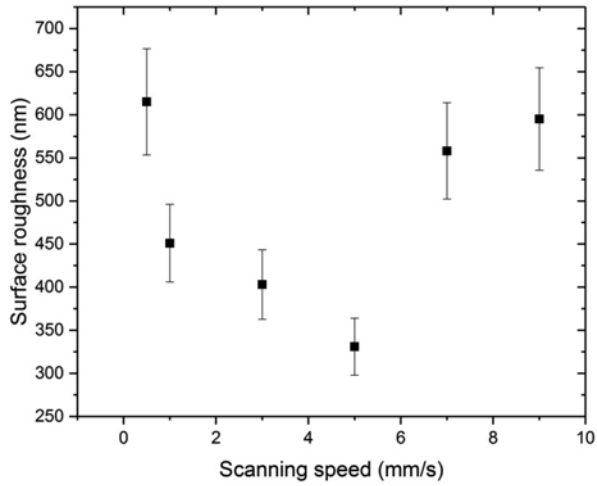

FIGURE 9
Graph of the cut surface of the 1.0 mm in thick quartz sheets cut with the femtosecond laser beam under 550 μJ pulse energy with different scanning speeds.

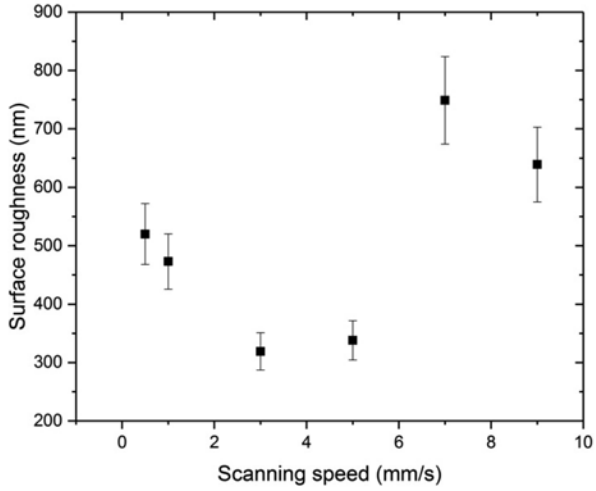

FIGURE 10
Graph of the cut surface of the 0.5 mm in thick quartz sheets cut with the femtosecond laser beam under 550 μJ pulse energy with different scanning speeds.

separated. A line trend was expected. When the scanning speed was slower than 1.7 mm/s, the pulses were overlapped, which generated heat accumulation, thus leading to overheating breaking the uniformity of the intensity of Bessel beam, and larger values of residual surface roughness; also, due to the larger ablation area on top surface, material near the top surface was not processed, which leads to the increase of bending force. At a scanning speed faster than 5.0 mm/s, the pulses were separated too much, leading to insufficient weakening within the laser-inscribed area, and a gradual increase in the resulting residual surface roughness as well as the bending force, as shown in Figure 6 and Figure 7. When the scanning speed was further increased above 10.0 mm/s, the risks of cleavage failure was increased. Cleavage could not be achieved along the Bessel beam scanning path. By decreasing the pulse energy to 400 μJ, as can be seen in Figure 11 and Figure 12, the lower pulse energy means less heat accumulation in low scanning speeds slower than 4.0 mm/s, so the surface roughness was not increased anymore. For higher scanning speeds faster than 4.0 mm/s the rising trend of the surface roughness still exists. To achieve high quality quartz cleavage, the lower sidewall roughness as well as the lower bending force are required. So, by using the optimized parameters of 4.0 mm/s scanning speed and 400 μJ pulse energy, quartz cutting and cleavage with right angle and rounded corners was achieved. At the same time, cuts with zero-width with no debris and microcracks on the cut surface were achieved, as is evident from Figure 13 and Figure 14.

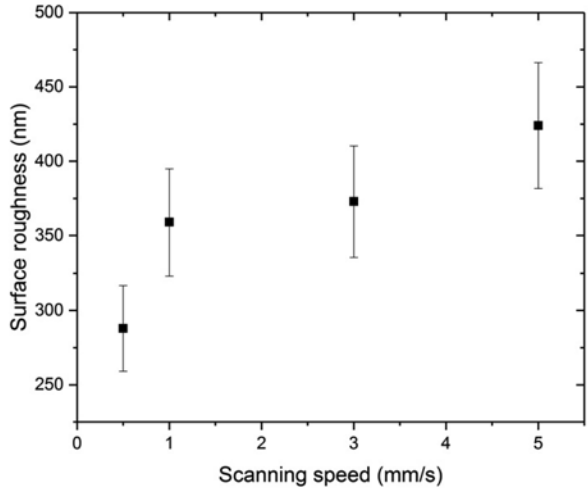

FIGURE 11
Graph of the cut surface of the 1.0 mm in thick quartz sheets cut with the laser at 400 μJ pulse energy with different scanning speeds.

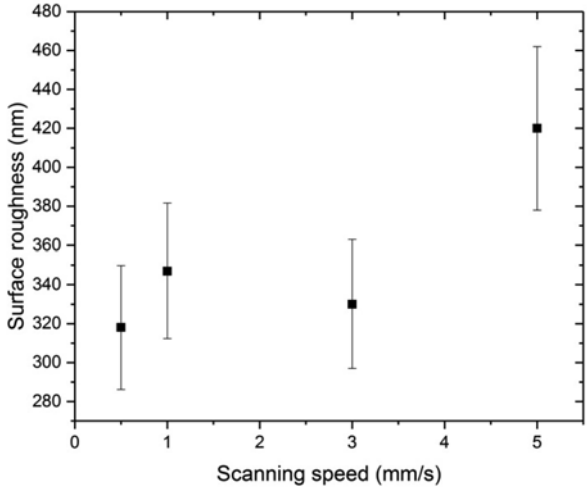

FIGURE 12
Graph of the cut surface of the 0.5 mm in thick quartz sheets cut with the laser at 400 μJ pulse energy with different scanning speeds.

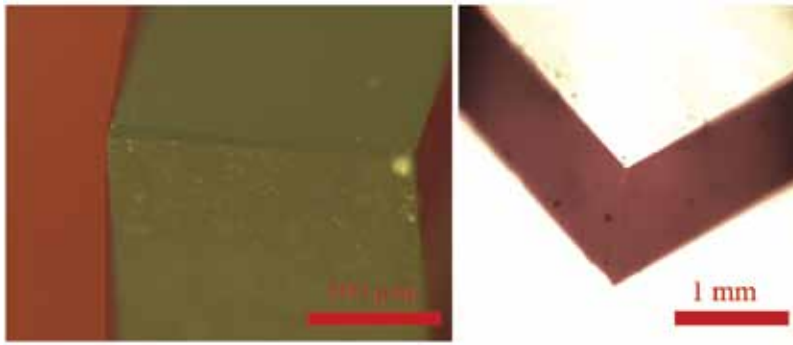

FIGURE 13
Optical micrographs obtained showing right angle cuts in the 1.0 mm thick quartz plates.

FIGURE 14
Photograph showing examples of 1.0 mm thick quartz sheet cut to round corners with radii of 2 and 4 mm and a right angle square structure cut with a side length of 16 mm.

4 CONCLUSIONS

High quality dicing of 1.0 mm thick quartz (JKS2) sheets has been achieved by using Ti:Sapphire femtosecond non-diffraction zero order Bessel beam filamentation. The Bessel beam was generated by using an axicon lens with a physical angle of 20.0°. Vertical wall dicing have been achieved with a zero cut kerf width and no debris and micro crack on the cut surface. The effects

of pulse energy and scanning speed on Bessel beam cutting, cleavage force and the sidewall surface roughness were discussed in this paper. Both right angle and round corner cutting have been realised and ultra low surface roughness (around 330 nm) was achieved.

ACKNOWLEDGMENT

This research was partially supported by the National Key R&D Program of China (2017YFB1104604).

NOMENCLATURE

L	Central core length of the Bessel beam (m)
n	Refractive index of the fused silica
r	Central core diameter of the Bessel beam (m)

Greek symbols

α	Physical angle of the axicon lens (^{o})
β	Deflection angle of the Bessel beam (^{o})
λ	Wavelength of laser beam (m)
ω_o	Illumited beam diameter (m)

REFERENCES

[1] Zhou M., Ngoi B.K.A., Yusoff M.N. and Wang X.J. Tool wear and surface finish in diamond cutting of optical glass. *Journal of Materials Processing Technology* **174**(1-3) (2006), 29–33.

[2] Yuan F., Allred D.D., Johnson J.A. and Todd R.H. Waterjet cutting of cross-linked glass. *Journal of Vacuum Science and Technology A: Vacuum, Surfaces and Films* **13**(1) (1995), 136–139.

[3] Prakash E.S., Sadashivappa K., Joseph V. and Singaperumal M. Nonconventional cutting of plate glass using hot air jet: Experimental studies. *Mechatronics* **11**(6) (2001), 595–615.

[4] Ueda T., Yamada K., Oiso K. and Hosokawa A. Thermal stress cleaving of brittle materials by laser beam. *CIRP Annals* **51**(1) (2002), 149–152.

[5] Strigin M.B. and Chudinov A.N. Cutting of glass by picosecond laser radiation. *Optics Communications* **106**(4-6) (1994), 223–226.

[6] Nisar S., Sheikh M.A., Li L. and Safdar S. The effect of material thickness, laser power and cutting speed on cut path deviation in high-power diode laser chip-free cutting of glass. *Optics & Laser Technology* **42**(6) (2010), 1022–1031.

[7] Varel H., Ashkenasi D., Rosenfeld A., Wahmer M. and Campbell E. Micromachining of quartz with ultrashort laser pulses. *Applied Physics A: Materials Science & Processing* **65**(4-5) (1997), 367–373.

[8] Ahmed F., Lee M.S., Sekita H., Sumiyoshi T. and Kamata M. Display glass cutting by femtosecond laser induced single shot periodic void array. *Applied Physics A: Materials Science & Processing* **93**(1) (2008), 189–192.

[9] Bovatsek J.M., Arai A.Y. and Yoshino F. *Transparent Material Processing with an Ultrashort Pulse Laser*. US Patent US 20070051706 A1, 8th September 2006.

[10] Hosseini S.A. and Herman P.R. *Method of Material Processing by Laser Filamentation*. European Patent EP2593266A2, 12th July 2011,

[11] Durnin J., Eberly J.H. and Miceli J.J. Comparison of Bessel and Gaussian beams. *Optics Letters* **13**(2) (1988), 79–80.

[12] Duocastella M. and Arnold C.B. Bessel and annular beams for materials processing. *Laser & Photonics Reviews* **6**(5) (2012), 607–621.

[13] Wang Y., Yan S., Friberg A.T., Kuebel D. and Visser T.D. Electromagnetic diffraction theory of refractive axicon lenses. *Journal of the Optical Society of America A: Optics, Image Science and Vision* **34**(7) (2017), 1201–1211.

[14] Dudutis J., Gečys P. and Račiukaitis G. Non-ideal axicon-generated Bessel beam application for intra-volume glass modification. *Optics Express* **24**(25) (2016), 28433–28443.

[15] Durnin J., Miceli J.J.J. and Eberly J.H. Diffraction-free beams. *Physical Review Letters* **58**(15) (1987), 1499–1501.

[16] Davis K.M., Miura K., Sugimoto N. and Hirao K. Writing waveguides in glass with a femtosecond laser. *Optics Letters* **21**(21) (1996), 1729.

[17] Bhuyan M.K., Courvoisier F., Lacourt P.A., Jacquot M., Salut R., Furfaro L. and Dudley J.M. High aspect ratio nanochannel machining using single shot femtosecond Bessel beams. *Applied Physics Letters* **97**(8) (2010), 081102.